J. Fluid Mech. (1982), *vol.* 115, *pp.* 411–426
Printed in Great Britain

Flutter of thin cylindrical shells in cross flow

By M. P. PAIDOUSSIS AND D. T.-M. WONG

Department of Mechanical Engineering, McGill University,
817 Sherbrooke Street West, Montreal, Quebec, Canada

(Received 24 December 1980 and in revised form 28 May 1981)

This paper presents an analytical model for the aeroelastic instability of an infinitely long cylindrical shell in cross flow. The mean flow field is represented by a free-streamline model, and the perturbation flow field by a velocity potential associated with deformation of the shell cross-section; motions of the shell are described by Flügge's two-dimensional equations. It is shown that certain types of shell motions induce a negative aerodynamic damping, which increases with flow velocity; for sufficiently high flow, it overcomes the positive dissipative damping of the system, precipitating flutter, sequentially in the second, third and higher circumferential modes of the shell – each with specific orientation of the nodal pattern with respect to the free-stream vector. These analytical predictions are in agreement with observations in wind-tunnel experiments; quantitatively, predicted and measured flow-velocity instability thresholds are of the same order of magnitude.

1. Introduction

Wind-induced ovalling, or 'breathing', oscillations of thin metal chimney stacks were first recorded in the 1950s (Dickey & Woodruff 1956, Dockstader, Swiger & Ireland 1956). In contrast to the well-known vortex-induced lateral oscillations of cylinders in cross flow, ovalling involves harmonic deformation of the shell cross-section, while the long axis of the shell remains stationary. Thus, in the course of ovalling in the nth circumferential mode, the radius r of a cylindrical shell, at an azimuthal position θ, varies as

$$r(\theta, t) = a(1 + \epsilon \cos n\theta e^{i\omega t}),$$

a being the radius of the undeformed circular cross-section, ϵa the maximum displacement from the mean position, and ω the circular frequency of oscillation. Third-mode oscillation ($n = 3$) is shown in figure 1(*a*). Etymologically, ovalling should strictly apply only to the second circumferential mode ($n = 2$), but the term is widely used for higher modes as well, i.e. for all $n \geqslant 2$.

It has been commonly held that ovalling oscillations are induced by the alternate vortices shed in the wake of the cylinder (Dockstader *et al.* 1956, Johns & Sharma 1974). The mechanism was supposed to be similar to that causing lateral oscillation at, or near, resonances between the vortex-shedding and natural frequencies of a cylinder in cross flow; in the case of ovalling, however, it was postulated to be sufficient that a condition of subharmonic resonance exist, i.e. that the vortex-shedding frequency be an integral submultiple of the ovalling frequency of the shell.

Recently, Paidoussis & Helleur (1979) have shown experimentally that this

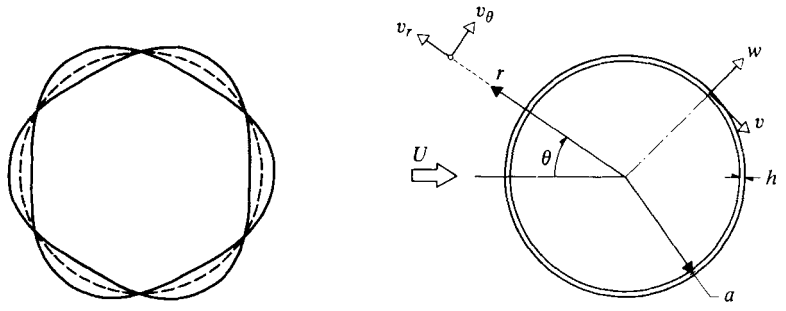

FIGURE 1. (*a*) Cross-sectional view of the third circumferential mode of oscillation, showing the two extreme positions of the middle surface of the shell in the course of a cycle of oscillation; (*b*) the system under consideration, defining various quantities used in the analytical model.

sub-harmonic relationship appears to exist only close to the onset of ovalling.† Beyond that point, the oscillation persists over a wide range of flow velocities, yet this relationship no longer holds; the ovalling frequency remains sensibly constant and close to the appropriate natural frequency of the shell, while the vortex-shedding frequency increases linearly with flow velocity, following a constant Strouhal-number relationship. Hence, it was concluded that, beyond the threshold of ovalling, the oscillation would have to be sustained by a mechanism other than synchronization with vortex shedding. Moreover, further experiments, by the same authors, with a long splitter plate behind the shell indicated that ovalling still occurs – albeit at a slightly higher velocity threshold – despite the fact that periodic vortex shedding had been suppressed. This demonstrates that, even at its onset, ovalling does not depend on the existence of any alternating periodicity in the wake.‡

With Paidoussis & Helleur's (1979) experiments it became clear that the mechanism underlying ovalling is different and more complex than had previously been supposed. It is in the context of the search for this mechanism that the present paper may be viewed; alternatively, it may be considered as a specific study of the behaviour of long, thin cylindrical shells in cross flow.

In this paper a theory is developed to study the stability of a thin elastic cylindrical shell in incompressible two-dimensional cross flow. It is obviously much simpler to examine this problem, rather than the more 'realistic' one involving a free end, thus eliminating the complexities of three-dimensional flow over the top. (Prudently, it was first confirmed in the laboratory that a shell spanning the wind tunnel and supported at both ends is also subject to ovalling.) In the model, it has been assumed that

† Actually, very recent, yet unpublished measurements by Suen (1981) indicate that, although an integral (or approximately integral) relationship between ovalling and vortex shedding does occur frequently, it is nevertheless often entirely absent, *even at the onset of ovalling*.

‡ One of the referees of this paper suggested the possibility of synchronous, symmetric vortex shedding from the two sides of the cylindrical shell, as yet another excitation mechanism through which ovalling oscillations could be induced by vortex shedding. This type of vortex shedding has been found to occur in conjunction with in-line oscillation of cylinders in cross flow (King, Prosser & Johns 1973). However, in a special set of experiments for testing this hypothesis, the authors found that vortex shedding – both before and after the onset of ovalling – is of the normal, antisymmetric type. (These experiments involved two hot-wire anemometers placed close to the separation points on either side of the shell; the phase difference in cross-spectral-density analysis of the two signals was found always to be approximately 180°.)

ovalling oscillation is entirely due to aeroelastic coupling between the shell and the fluid, independently of any periodicity due to vortex shedding in the wake, the existence of which is entirely ignored.

2. Theory

General approach

In this analysis, the shell is first idealized to be infinitely long, so that the problem may be treated as two-dimensional. The cross flow is further simplified by regarding the entire field as quasi-irrotational. The wake is separated from the outer flow by a dividing streamline. Within the wake, the von Kármán vortex street will be totally ignored, giving a zero flow velocity in this region. Hence, the flow field is assumed to be steady, except for the disturbances arising from the vibration of the shell. Moreover, it is assumed that the time-averaged positions of separation of the mean flow from the body surface are unaffected by the small vibrations of the shell. The effect of turbulence is ignored throughout.

The shell is considered to be purely elastic, homogeneous and isotropic. To study its stability, a small-amplitude vibration in a given circumferential mode is imposed on the shell. As this study is principally concerned with the *onset* of ovalling, the vibration amplitude is taken to be sufficiently small, to allow linear shell theory and linearized fluid mechanics to be utilized. In the same spirit, the boundary conditions on the shell surface will be applied at the equilibrium position.

In its essence, the analysis determines the perturbation flow field associated with shell motions, and then the resultant pressure fluctuations on the shell surface, the effect of which would indicate whether the initial vibration is attenuated or amplified.

In addition to this analysis, involving an infinitely long shell, an analytical model has been developed for a finite shell with clamped ends in two-dimensional cross flow. This model is considerably more complex, insofar as the equations of motion of the shell are concerned, yet provides no additional insight into the problem; hence, although some numerical results of that analysis will be given, the details will not be presented in this paper.

Equations of motion and boundary conditions

Consider a uniform thin cylindrical shell of infinite length, mean radius a and thickness h, subjected to a uniform cross flow of incident velocity U, as shown in figure 1 (*b*); the shell is filled with stationary fluid of the same density as the outer flow. As the problem is two-dimensional, only planar displacements of the middle surface of the shell, in the plane of figure 1, are considered: $v(\theta, t)$ and $w(\theta, t)$, in the circumferential and radial directions, respectively, measured from the equilibrium (circular) configuration.

In this case, the equations of motion of a shell of density ρ_s, Young's modulus E, and Poisson's ratio ν, according to Flügge (1957) reduce to

$$\frac{\partial^2 v}{\partial \theta^2} + \frac{\partial w}{\partial \theta} = \gamma \frac{\partial^2 v}{\partial t^2}, \tag{1}$$

$$\frac{\partial v}{\partial \theta} + w + \kappa \left\{ \frac{\partial^4 w}{\partial \theta^4} + 2 \frac{\partial^2 w}{\partial \theta^2} + w \right\} = -\gamma \left\{ \frac{\partial^2 w}{\partial t^2} - \frac{q_r}{\rho_s h} \right\}, \tag{2}$$

where $\kappa = h^2/12a^2$, $\gamma = \rho_s a^2(1-\nu^2)/E$ and $q_r = p_i - p_e$, p_i and p_e being respectively the internal and external pressure on the shell surface.

These equations being linear, the pressure difference q_r may be separated into two components: $q_{r_0}(\theta)$, which is due to the static loading of the mean flow, and $q_r^*(\theta, t)$, which is due to perturbations associated with shell deformations characterized by $v^*(\theta, t)$ and $w^*(\theta, t)$. Considering deformations associated with $q_{r_0}(\theta)$ to be negligible,† (1) and (2) may be viewed as relationships among q_r^*, v^* and w^*, from which the static components have been filtered out.

Since the flow field is assumed to be irrotational outside the wake, a velocity potential $\Phi(r, \theta, t)$ may be defined by

$$v_r = \frac{\partial \Phi}{\partial r}, \quad v_\theta = \frac{1}{r}\frac{\partial \Phi}{\partial \theta},$$

where $v_r(r, \theta, t)$ and $v_\theta(r, \theta, t)$ are respectively the radial and tangential velocities at position (r, θ). As Φ must satisfy Laplace's equation, which is linear, one may further let

$$\Phi(r, \theta, t) = \phi_0(r, \theta) + \phi^*(r, \theta, t),$$

where $\phi_0(r, \theta)$ is associated with the mean flow, and $\phi^*(r, \theta, t)$ with the perturbation flow field, due to oscillations of the shell. Once $\Phi(r, \theta, t)$ is known, the pressure may be determined from Bernoulli's equation for unsteady flow,

$$\frac{\partial \Phi}{\partial t} + \tfrac{1}{2}V^2 + \frac{p}{\rho} = 0, \tag{3}$$

where p is the static pressure measured relative to the stagnation pressure of the free stream, ρ is the fluid density, and $V^2 = v_r^2 + v_\theta^2$; the term $F(t)$ normally appearing on the right-hand side of (3) may be suppressed for incompressible flow (Lamb 1957) – or alternatively may be considered to have been absorbed in $\partial\Phi/\partial t$.

It is noted that ϕ_0 is associated entirely with the external flow, and may be defined in terms of the radial and tangential velocities on the surface of a stationary cylinder, i.e.

$$\left.\frac{\partial \phi_0}{\partial r}\right|_{r=a} = 0, \quad \left.\frac{1}{a}\frac{\partial \phi_0}{\partial \theta}\right|_{r=a} = Uf(\theta),$$

where $f(\theta)$ may be determined empirically, or by semi-empirical methods such as that developed by Parkinson & Jandali (1969). According to all reported cases, ovalling experiences have occurred in the Reynolds-number range $Re = 10^4$–10^6; hence the boundary-layer thickness on the shell prior to separation is sufficiently thin for the pressure change across it to be negligible. The local steady-state velocity just outside the boundary layer may then be related to the surface static pressure p by Bernoulli's equation for the steady flow, so that

$$f(\theta) \equiv \{v_\theta|_{r=a}/U\} = (1 - C_p)^{\frac{1}{2}} \quad \text{for} \quad |\theta| \leqslant \beta_s, \tag{4}$$

where C_p is the pressure coefficient defined by

$$C_p = (p - p_\infty)/\tfrac{1}{2}\rho U^2,$$

† For the shells used in the experiments, bearing in mind their length/radius and thickness/radius ratios, this may be considered to be supported by experimental evidence: the natural frequencies of oscillation of the shell with and without flow are essentially the same.

in terms of the free-stream static pressure p_∞, and where β_s is the angular position of the point of separation. In the wake, the surface flow may be considered to be negligible so that

$$f(\theta) = 0 \quad \text{for} \quad \pi \geqslant |\theta| > \beta_s. \tag{5}$$

In this paper, $f(\theta)$ was determined empirically in terms of the measured C_p for a rigid cylinder in cross flow. For example, using Roshko's (1954) data for $Re = 1{\cdot}45 \times 10^4$ and employing a least-square-fit technique, $f(\theta)$ may be approximated by the fourth-order polynomials

$$f(\theta) = 1{\cdot}6073|\theta| + 0{\cdot}5700|\theta|^2 - 0{\cdot}9394|\theta|^3 + 0{\cdot}1714|\theta|^4$$
$$\text{for} \quad |\theta| \leqslant 1{\cdot}484 \text{ rad } (85°), \tag{6}$$

$$f(\theta) = 1{\cdot}5137|\theta| + 0{\cdot}5128|\theta|^2 - 0{\cdot}9418|\theta|^3 + 0{\cdot}1733|\theta|^4$$
$$\text{for} \quad |\theta| \leqslant 1{\cdot}396 \text{ rad } (80°), \tag{7}$$

for a cylinder without and with a splitter plate, respectively. It is noted that, as one would expect, the flow is symmetric relative to the stagnation point ($\theta = 0$).

Turning next to the perturbation velocity potential ϕ^* it is noted that it has components associated with both internal and external fluids, ϕ_i^* and ϕ_e^* respectively. In view of (3), the former gives rise to pressure fluctuations

$$p_i^* = -\rho \frac{\partial \phi_i^*}{\partial t}\bigg|_{r=a},$$

and the latter to

$$p_e^* = -\rho \left\{ \frac{\partial \phi_e^*}{\partial t} + \frac{Uf(\theta)}{a} \frac{\partial \phi_e^*}{\partial \theta} \right\}\bigg|_{r=a},$$

correct to first order of small quantities, having introduced the approximation $V^2 \simeq U^2 f^2(\theta) + 2Uf(\theta)\, a^{-1} (\partial \phi_e^* / \partial \theta)|_{r=a}$.†

Finally, ϕ_i^* and ϕ_e^* may be related to the shell deformation. For a fluid particle on the outer surface of the shell, the radial velocity is given by

$$\frac{\partial \phi_e^*}{\partial r}\bigg|_{r=a} = \frac{Dw^*}{Dt} \simeq \frac{\partial w^*}{\partial t} + \frac{1}{a} v_\theta \bigg|_{r=a} \frac{\partial w^*}{\partial \theta};$$

assuming that $Uf(\theta) \gg (\partial \phi_e^* / a\, \partial \theta)|_{r=a}$, this may be simplified further to

$$\frac{\partial \phi_e^*}{\partial r}\bigg|_{r=a} = \frac{\partial w^*}{\partial t} + \frac{Uf(\theta)}{a} \frac{\partial w^*}{\partial \theta}. \tag{8}$$

Similarly, for the internal fluid

$$\frac{\partial \phi_i^*}{\partial r}\bigg|_{r=a} = \frac{\partial w^*}{\partial t}. \tag{9}$$

† Of course, it is realized that the mean-flow component of (3), after (4) and (5) have been substituted in it, is incorrect, as it corresponds to a mean pressure distribution such that the pressure in the wake is effectively equal to the stagnation pressure. This relation, however, is not used (nor is it useful) in this analysis, the assumption having been made that the steady pressure field induces no appreciable deformation of, nor stresses in, the shell.

3. Analysis

For harmonic shell motions, it may be assumed that

$$\phi^* = R(r)\,T(\theta)\,e^{i\omega t},$$

which substituted into Laplace's equation, in cylindrical co-ordinates, gives

$$\frac{r^2}{R}\frac{d^2R}{dr^2}+\frac{r}{R}\frac{dR}{dr} = -\frac{1}{T}\frac{d^2T}{\partial\theta^2} = \lambda^2,$$

where λ^2 has to be a positive integer in order to satisfy the condition $\phi^*(\theta) = \phi^*(\theta+2\pi)$. Hence

$$T(\theta) = A_1\cos\lambda\theta + A_2\sin\lambda\theta,$$

for some constants A_1 and A_2, to be determined.

So far, all observations on the ovalling process have revealed that, independently of the circumferential mode excited, either a node or an antinode faces the free stream. Therefore the analysis will be restricted to conform to either of these two observed conditions. For the type of oscillation with an antinode facing the free stream, the symmetry of the flow field would render

$$v_\theta|_{\theta=0} = Uf(0)+\frac{1}{a}\frac{\partial\phi_e^*}{\partial\theta}\bigg|_{r=a,\theta=0} = 0,$$

and, in view of the symmetry of the steady cross flow, $f(0) = 0$, leading to

$$(\partial\phi_e^*/\partial\theta)|_{r=a,\theta=0} = 0.$$

This clearly implies that

$$T(\theta) = A_1\cos\lambda\theta$$

for such configurations. The cases with a node facing the free stream may be tackled in very similar fashion, as highlighted in the appendix.

Now, it may easily be seen that

$$R(r) = Dr^{-\lambda}+Er^{\lambda},$$

for some constants D and E. Physically, one would expect $\phi_e^* \to 0$ as $r \to \infty$ and ϕ_i^* to be finite at $r = 0$. Hence, the perturbation potential, external and internal to the shell, must take the form

$$\phi_e^* = e^{i\omega t}\sum_{\lambda=0}^{\infty} D(\lambda)\,r^{-\lambda}\cos\lambda\theta, \tag{10}$$

$$\phi_i^* = e^{i\omega t}\sum_{\lambda=0}^{\infty} E(\lambda)\,r^{\lambda}\cos\lambda\theta. \tag{11}$$

To proceed with determining $D(\lambda)$ and $E(\lambda)$, w^* is expanded in series form

$$w^* = e^{i\omega t}\sum_{l=0}^{\infty} B_l\cos(2l+1)\,n\theta, \tag{12}$$

so chosen that the number of nodal points for the nth mode be $2n$, as required. Consequently, v^* must have the similar form

$$v^* = e^{i\omega t}\sum_{l=0}^{\infty} A_l\sin(2l+1)\,n\theta. \tag{13}$$

Now, substitution of (12) and (10) into (8) yields

$$\sum_{l=1}^{\infty} \lambda D(\lambda)\, a^{-\lambda-1} \cos \lambda\theta = \frac{Un}{a} f(\theta) \sum_{l=0}^{\infty} B_l (2l+1) \sin (2l+1)\, n\theta - i\omega \sum_{l=0}^{\infty} B_l \cos (2l+1)\, n\theta.$$

For a particular $\lambda = \lambda_j$, one may solve for $D(\lambda_j)$ by multiplying both sides by $\cos \lambda_j \theta$ and integrating over θ from 0 to π, whereby it may be shown that

$$D(\lambda) = \frac{-2}{\pi} \frac{a^{\lambda+1}}{\lambda} \left\{ \tfrac{1}{2} i\omega\pi \sum_{l=0}^{\infty} B_l \delta_{\lambda b} - \frac{U}{a} \sum_{l=0}^{\infty} B_l b \int_0^{\pi} \sin b\theta \cos \lambda\theta f(\theta)\, d\theta \right\}, \tag{14}$$

for $\lambda = 1, 2, 3, \ldots$, where $b = (2l+1)\, n$ and $\delta_{\lambda b}$ is the Kronecker delta. $D(0)$ is arbitrary, since only the derivative of ϕ_e^* is specified at the boundary.

By similar means one may obtain

$$E(\lambda) = \frac{i\omega}{\lambda} a^{1-\lambda} B_l \delta_{\lambda b}, \tag{15}$$

for $\lambda = 1, 2, 3, \ldots$.

From (10) and (14) it is obvious that p_e^* will be specified in terms of a double series, and some simplification is desirable before proceeding further with the analysis. Fortunately, the modal shapes are adequately described by the leading terms in the series of (12) and (13), suggesting

$$w^* = e^{i\omega t} B_0 \cos n\theta, \quad v^* = e^{i\omega t} A_0 \sin n\theta; \tag{16), (17}$$

the validity of this approximation was tested *a posteriori* by repeating the analysis with a three-term approximation; the difference in the results was found to be negligible. Then, letting $p^* = P^* e^{i\omega t}$, one obtains

$$P_e^* = \rho B_0 \left\{ \frac{2}{\pi} \frac{U^2 n}{a} f(\theta) \sum_{\lambda=1}^{\infty} F_1(\lambda) \sin \lambda\theta - Ui\omega f(\theta) \sin n\theta \right.$$
$$\left. - \frac{2}{\pi} i\omega U n \sum_{\lambda=1}^{\infty} \frac{F_1(\lambda)}{\lambda} \cos \lambda\theta - \frac{\omega^2 a}{n} \cos n\theta \right\} - \rho i\omega D(0), \tag{18}$$

$$P_i^* = \rho B_0 \omega^2 \frac{a}{n} \cos n\theta - \rho i\omega E(0), \tag{19}$$

where

$$F_1(\lambda) = \int_0^{\pi} f(\xi) \sin n\xi \cos \lambda\xi\, d\xi.$$

Finally, substituting (16)–(19) into (1) and (2) yields two equations of the form

$$a_{11} A_0 + a_{12} B_0 = 0, \quad a_{21} A_0 + a_{22} B_0 = 0,$$

where

$$a_{11} = n^2 - \gamma\omega^2, \quad a_{12} = n, \quad a_{21} = \tfrac{1}{2} n\pi,$$

$$a_{22} = \tfrac{1}{2}\pi \{1 + \kappa(n^2-1)^2 - \gamma\omega^2\} + \frac{\gamma}{\rho_s h} \left\{ -\rho \frac{a\pi}{n} \omega^2 - 2\rho U F_1(n)\, i\omega + \rho U^2 \frac{2n}{\pi a} \sum_{\lambda=1}^{\infty} F_1(\lambda)\, F_2(\lambda) \right\},$$

and $F_2(\lambda) = \int_0^{\pi} f(\xi) \sin \lambda\xi \cos n\xi\, d\xi$. For non-trivial solutions of A_0 and B_0, the associated determinant must vanish, giving the characteristic equation for the frequency ω – which will generally be complex.

The foregoing analysis applies to shell deformations such that an antinode faces

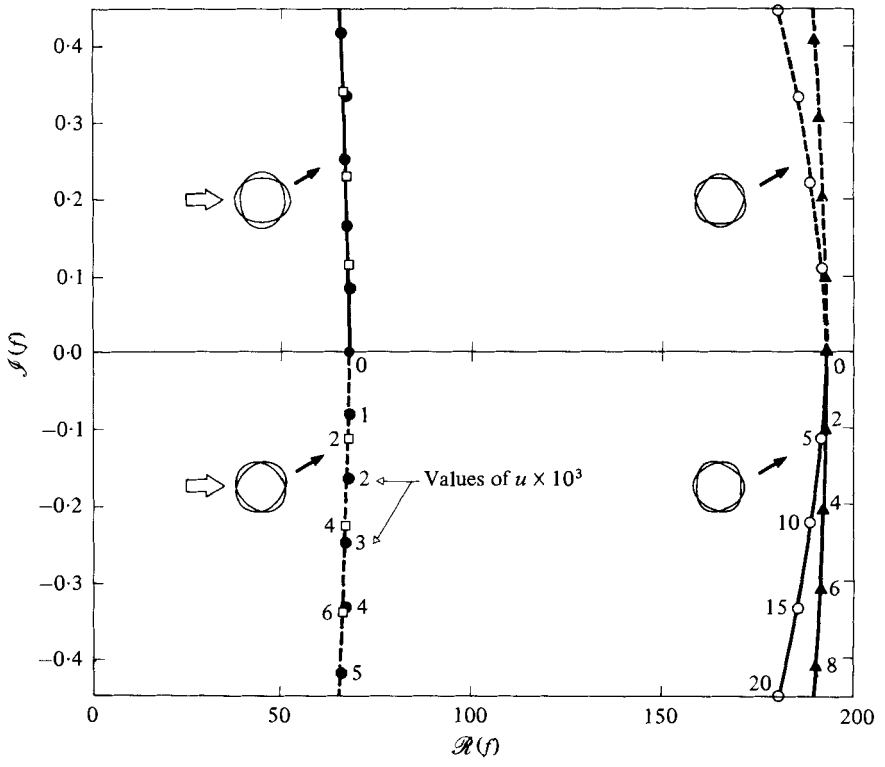

FIGURE 2. Argand diagram of the complex frequencies f of the second and third modes of an infinitely long shell in cross flow, as functions of the dimensionless flow velocity u. ●, 2nd mode, no splitter plate; □, 2nd mode, splitter plate; ▲, 3rd mode, no splitter; ○, 3rd mode, splitter.

the free stream. Using a similar approach, the case of a node facing the stream has also been investigated. To avoid unnecessary duplication, only an outline of the necessary changes in the analysis is given here, in the appendix.

4. Theoretical results

Calculations were conducted for an infinitely long shell of radius, thickness and material properties identical with one of the shells tested in the experiments to be discussed next, namely $a = 38{\cdot}1$ mm, $h = 0{\cdot}51$ mm, $E = 0{\cdot}28 \times 10^{10}$ N/m^2, $\rho_s = 1{\cdot}29 \times 10^3$ kg/m^3 and $\nu = 0{\cdot}4$. The complex frequencies $f(\equiv \omega/2\pi)$ [in Hz] of the second and third circumferential modes are shown in figure 2 in the form of an Argand diagram, for increasing dimensionless flow velocity u, defined by

$$u = U\{\rho_s(1-\nu^2)/E\}^{\frac{1}{2}}.$$

Referring now to figure 2, it is noted that, as internal dissipation (material damping) has not been included in the theoretical model, the frequencies at $u = 0$ are wholly real. For $u > 0$, however, it is seen that second-mode oscillation ($n = 2$) with a node facing the stream is associated with a *negative* aerodynamic damping, i.e. $\mathscr{I}(f) < 0$; if, on the other hand, an antinode faces the stream, the motion is aerodynamically

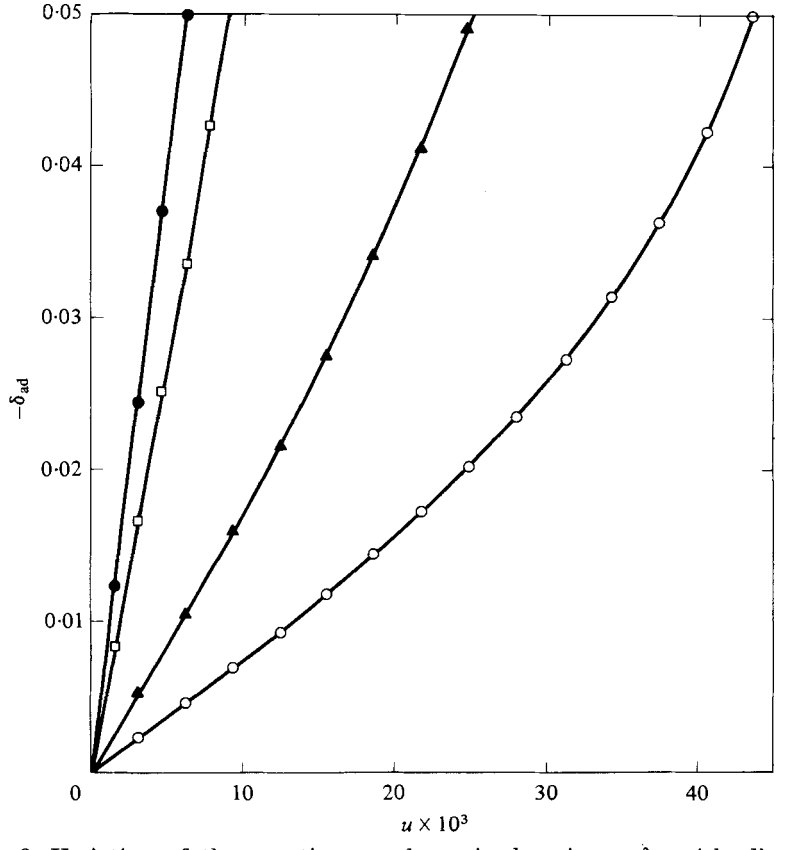

FIGURE 3. Variation of the negative aerodynamic damping $-\delta_{ad}$ with dimensionless flow velocity u for the second and third modes of an infinitely long shell in cross flow. Symbols as in figure 2.

positively damped. The opposite is true for third-mode ($n = 3$) oscillations. It is also seen that similar results obtained in the two cases, without and with a splitter plate, except that in the latter case $|\mathscr{I}(f)|$ is generally smaller.

These results may be interpreted as follows. With increasing flow velocity the vibration frequencies remain almost constant, as the values of $\mathscr{R}(f)$ for $u > 0$ are only slightly lower than the corresponding ones for $u = 0$. The aerodynamic damping, however, conveniently characterized by the logarithmic decrement $\delta_{ad} = 2\pi\mathscr{I}(f)/\mathscr{R}(f)$ increases almost linearly with u, as shown in figure 3. For sufficiently high flow velocity, the negative aerodynamic damping associated with each of the two modes will eventually exceed the corresponding dissipative-modal-damping logarithmic decrement, δ_{md}; at that point the net energy transfer from the fluid to the shell exceeds the energy lost through dissipation, and oscillations will be amplified, i.e. this is the threshold of instability in the mode concerned.

Thus, the mechanism of instability is recognized as being that of single-degree-of-freedom flutter, rather than the so-called 'classical' two-degree, or coupled-mode flutter (Dowell 1975; Scanlan 1981*a*, *b*). The latter arises through aerodynamic 'stiffness' terms, causing the frequencies of two modes of the system, initially different at zero flow, to coincide (coalesce) at some given flow velocity; this gives rise to

instability due to coupling of the two modes.† In contrast, the instability obtained by this analysis is associated with the aerodynamic 'damping' terms, where the system becomes unstable in one of its modes when the aerodynamic damping forces associated with motions in that one mode become negative and sufficiently large to overcome the structural dissipative forces – at which point the system loses stability as described in the paragraph above.‡

As an illustration of how figure 3 may be utilized, consider the case where the modal damping $\delta_{md} = 0{\cdot}02$ for both $n = 2$ and $n = 3$. Then, as the threshold of flutter occurs when $\delta_{md} = -\delta_{ad}$, one obtains, with the aid of figure 3, the critical flow velocities associated with second- and third-mode flutter, namely $u_c^{(2)} = 2{\cdot}50$ and $u_c^{(3)} = 11{\cdot}75$.

In summary, the results obtained in this section indicate that:

(i) shell flutter is possible in the absence of any periodicity in the wake of the shell;

(ii) for the two modes involved, second-mode flutter should develop with a node facing upstream, while third-mode flutter with an antinode facing upstream;§

(iii) if modal damping in the two modes is similar, second-mode flutter should occur at a lower flow velocity than third-mode flutter,‖

(iv) the critical flow velocities, $u_c^{(2)}$ and $u_c^{(3)}$, are raised somewhat by the presence of a splitter plate in the wake.

5. Experiments

General description

The experiments were conducted in a low-speed, open-return, suction wind tunnel with a closed working section (Wygnanski & Newman 1961), 0·91 m (3 ft) wide and 0·61 m (2 ft) high. The cylindrical shells were spin-cast from low-viscosity epoxy material, with less than 3 % variation in wall thickness. They were mounted in the wind tunnel as shown in figure 4. Each end of the shell was clamped to a rigid cylindrical support, which was properly sealed. Care was taken to avoid any axial loading on the shell while mounting it into place.

The flow velocity was measured by standard means and has been corrected for tunnel blockage by Maskell's (1965) correction, which amounts to 5 % for shells 76·2 mm in diameter. The amplitude and frequencies of vibration of the shell were registered by a fibre-optics 'Fotonic' sensor, mounted inside the shell so as not to disturb the flow around the shell. It was normally directed towards the front stagnation

† The question may fairly be put as to whether classical flutter is also possible for the problem at hand, in addition to single-mode flutter. It may be postulated that the second and fourth circumferential modes, suitably superposed, could give rise to classical flutter, if their frequencies coalesce or, alternatively, in this special case, if their frequencies are in the ratio of 1:2. However, neither of these frequency relationships was found to obtain in the experiments – nor, for that matter, was it predicted by the theoretical model.

‡ It may be of interest to the reader to digress at this point, so as to point out that according to current thinking 'classical' flutter is considered to be rather rarer, and single-mode flutter rather more common, than was hitherto thought to be the case (Scanlan 1981*a*, *b*). In this connection, it is of interest that the Takoma Narrows bridge collapse, traditionally considered as the most dramatic illustration of failure due to classical flutter, is now attributed to single-degree-of-freedom torsional flutter (Scanlan 1981*a*, *b*).

§ Indeed, it is shown that all even-numbered and odd-numbered modes follow the pattern exemplified by the second and the third.

‖ It is noted, however, that linear theory is valid up to where the system first loses stability, and strictly not beyond that point.

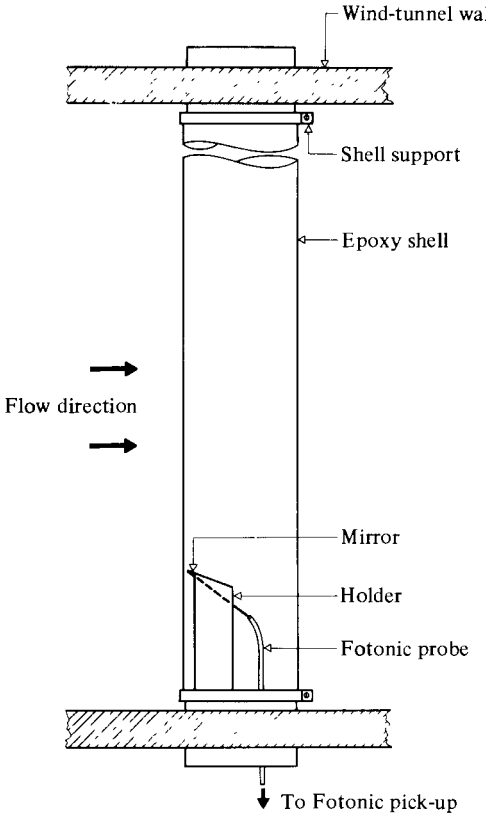

FIGURE 4. Schematic of the experimental set-up.

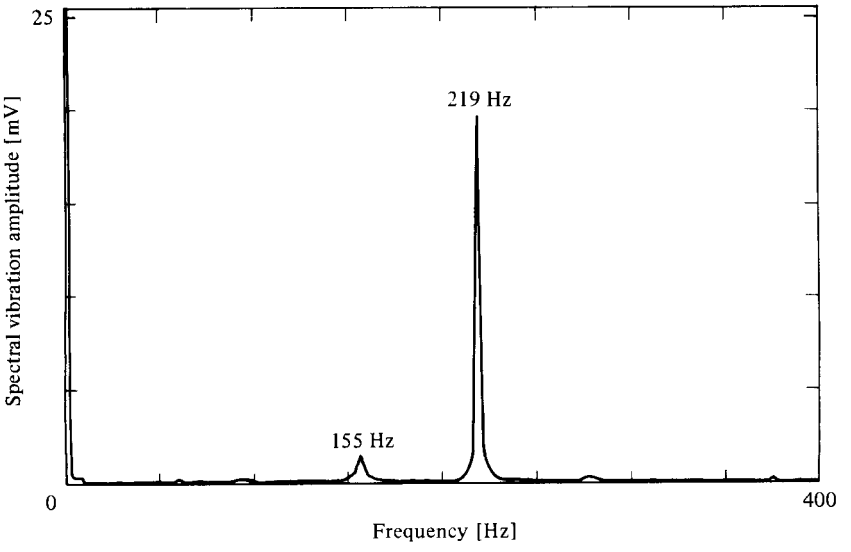

FIGURE 5. Frequency spectrum of the Fotonic-sensor signal at a flow velocity of 22 m/s.

Circumferential mode number n	Natural frequency $\mathscr{R}(f)$ [Hz]	Damping logarithmic decrement δ_{md}
2	155	0·031
3	225	0·034

TABLE 1. The natural frequencies and modal damping of the shell tested. The natural frequencies given here are those associated with the first axial mode of the shell.

point, or 45° to it, but could be rotated to locate the nodes and antinodes of vibration and hence the orientation of the modal shapes. Wake periodicity was also monitored, by a hot-wire anemometer placed downstream of the shell at a distance three-and-a-half times the shell diameter.

Both the hot-wire and Fotonic-sensor signals were sampled continuously by a Hewlett-Packard 5420A digital signal analyser. The dominant frequencies could readily be displayed in the form of a power-spectral density, such as shown in figure 5.

The normal experimental procedure was to increase the flow in the tunnel gradually, while monitoring shell vibration on the digital signal analyser, until a measurable coherent vibration was noticed. At this point, the flow velocity was measured, and the analysed signals from the Fotonic sensor and hot-wire anemometer were recorded. The flow velocity was then incremented and the same measurements taken, up to a maximum flow dictated by excessive shell vibration. Measurements below the threshold of vibration were also made.

To investigate the effect of periodic vortex shedding on ovalling, the experiments, which were first done without a splitter plate, were repeated with one (36·4 cm long, 0·16 cm thick) placed downstream of the shell and as close to it as practicable.

Observations and results

A detailed description of the experiments and of the results obtained will be given in a subsequent paper. Here the experiments conducted with only one specific, but typical, shell will be outlined briefly, to allow comparison with theory. The geometry and material properties of the shell were as given in § 4, except that it was of finite length (56·4 cm between supports) rather than infinitely long.

Prior to testing with flow, the natural frequencies of the shell and modal damping were measured *in situ* with the wind turned off. The results are summarized in table 1.

It should be mentioned that the measured natural frequencies agree with values calculated by the method outlined by Blevins (1979) to within 5 %. Damping was measured by an impedance technique utilizing Nyquist plots (Ray, Bert & Egle 1969; Ewins 1975).

The following observations were made with increasing wind speed. A coherent oscillation of 155 Hz was first observed at $U = 17{\cdot}3$–$17{\cdot}9$ m/s ($u = 5{\cdot}4 \times 10^{-3}$–$5{\cdot}6 \times 10^{-3}$), which was confirmed to be in the second mode, with a node facing upstream; the amplitude of this mode increased, reached a maximum and then decreased, while at $U = 20{\cdot}8$–$21{\cdot}4$ m/s ($u = 6{\cdot}5 \times 10^{-3}$–$6{\cdot}7 \times 10^{-3}$) a 225 Hz frequency appeared, which eventually became dominant; this was found to be associated with the third mode, with an antinode facing upstream. The results of one such typical run are shown in figure 6(*a*). Similar results for a nominally identical shell, but with average wall thickness 5 % smaller, are shown in figure 6(*b*).

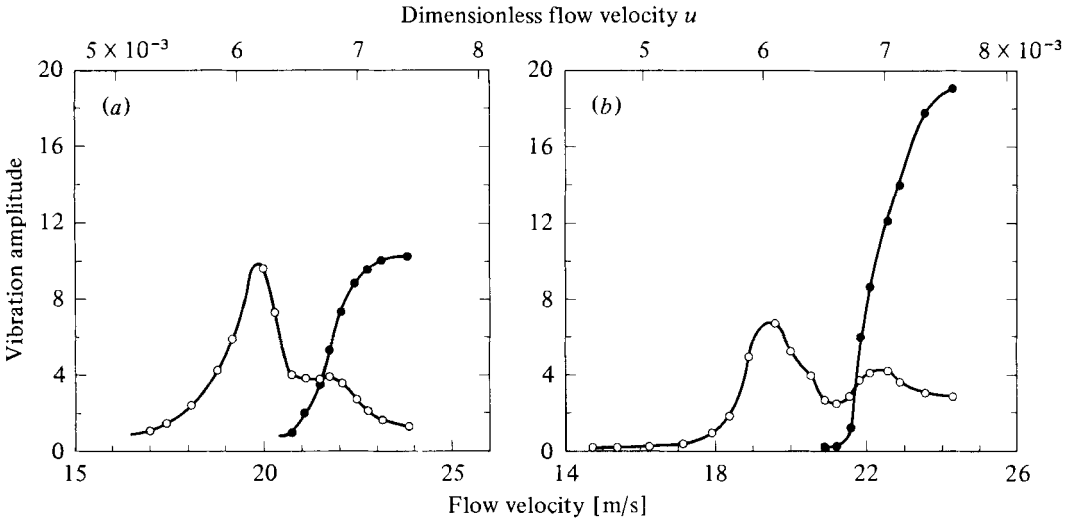

FIGURE 6. The amplitude of vibration (arbitrary scale) of two nominally identical shells, 56·4 cm long and clamped at both ends, in cross flow. The measured logarithmic decrements for the second and third mode, respectively, are (*a*) $\delta_2 = 0{\cdot}031$, $\delta_3 = 0{\cdot}042$, and (*b*) $\delta_2 = 0{\cdot}031$, $\delta_3 = 0{\cdot}034$; other dimensions and physical properties are given in the text. ○, 2nd mode; ●, 3rd mode.

The natural frequencies remained sensibly constant with increasing flow – generally varying by less than 2–3 %.†

It is noted that the oscillation amplitude in these figures was obtained with the Fotonic sensor pointing 45° to the free stream; hence, third-mode amplitudes are relatively higher than indicated. The amplitude scale is arbitrary, but the readings are linearly proportional to radial displacement; the maximum amplitude attained before the test was discontinued – for fear of damaging the shells – was of the order of $0{\cdot}2a$, a being the radius of the shell.

With the splitter plate in position, periodic vortex shedding was inhibited, as revealed by the hot-wire signal. However, the vibration characteristics remained the same, except that the critical flow velocities were raised somewhat, to $U_c^{(2)} \simeq 20{\cdot}4$ m/s and $U_c^{(3)} \simeq 24{\cdot}5$ m/s.

It should finally be noted that the thresholds of instability are in the Reynolds-number range of $Re \simeq 4 \times 10^4$; this is not far from the value in Roshko's experiments, from which equations (6) and (7) of the theory have been obtained, so that comparison between theory and experiment is meaningful (Goldstein 1952).

† In this connection, it should be noted that there were additional small differences in frequencies between one test run and another, arising from (*a*) manufacturing discrepancies among nominally identical shells, (*b*) lack of total repeatability in mounting the shells in the wind tunnel, and (*c*) temperature and humidity effects. These, together with the flow effect noted above, rarely exceeded 5 %; they are reflected in the small differences in the frequencies given in the various tables and figures of this paper.

	n	u_c	δ_{md}(expt)	$-\delta_{ad}$(theory)
Without splitter plate	2	$5{\cdot}5 \times 10^{-3}$	0·031	0·044
	3	$6{\cdot}6 \times 10^{-3}$	0·034	0·011
With splitter plate	2	$6{\cdot}3 \times 10^{-3}$	0·031	0·033
	3	$7{\cdot}6 \times 10^{-3}$	0·034	0·005

TABLE 2. Comparison of the negative aerodynamic damping $-\delta_{ad}$ with modal damping δ_{md} at the measured critical-flow velocities

6. Comparison between theory and experiment

Theory and experiment may strictly be compared only in a qualitative sense, as the former applies to infinitely long shells and the latter to shells with clamped ends and finite length. Nevertheless, reviewing the observations made in § 5, it is clear that the theoretical predictions (i)–(iv) of § 4 are qualitatively supported in full.

A quantitative comparison was also attempted, in table 2, in which the negative aerodynamic damping $-\delta_{ad}$ at the threshold of flutter is compared to the modal damping δ_{md}; according to theory the two should be equal. It is seen that δ_{md} and $-\delta_{ad}$ are generally of the same order of magnitude, especially the values associated with second-mode flutter, where linear theory should be expected to do best, as the system first loses stability in that mode. However, it is noted that, while theoretical and experimental third-mode frequencies $\mathscr{R}(f)$ are reasonably close (193 *vs.* 225 Hz), second-mode frequencies are in gross disagreement: 68 *vs.* 155 Hz. This, of course, reflects the difference in boundary conditions between theory and experiment; it does nevertheless cast doubt on the validity of the comparison of table 2.

To effect a more realistic comparison, a three-dimensional theoretical model was constructed, as mentioned in § 2. The fluid forces on the shell are determined by essentially the same method as before, by the use of 'strip theory',† but the shell is now considered to have a finite length and clamped ends. As a result, the shell equations and their solution become more complex, and details of this model are most likely of no great interest to the readers of this paper. However, some of the results obtained with this model *are* of interest: in table 3, the frequencies of oscillation and logarithmic decrements at the measured critical flow velocities are compared, similarly to table 2. As might be expected, by taking account of the actual end conditions of the shell, theory is more successful in predicting the oscillation frequencies. At the same time, it is noted that the theoretical $-\delta_{ad}$ have not come closer to the experimental values of δ_{md} – but they remain of the same order of magnitude.

In the above discussion, comparison between theory and experiment was made in terms of the experimental δ_{md} and the theoretical $-\delta_{ad}$, which emphasizes the basic mechanism of instability involved, as discussed in § 4. One could equally well compare theoretical to experimental critical flow velocities. Thus, for the results of table 3,

† According to strip theory, the fluid forces *at each axial location* x of the shell are still determined by the two-dimensional theory presented here; however, as perturbation pressures and forces depend on the local shell deformations, which in turn are functions of x, and hence of the axial-modal shape, strip theory yields an adequate approximation to the three-dimensional fluid forces. Of course, this approximation remains reasonable only so long as variations of shell displacements along the x-axis are small, so that the induced axial flow may be neglected.

	$\mathscr{R}(f)$ [Hz]			
n	Expt	Theory	δ_{md} (expt)	$-\delta_{ad}$ (theory)
2	155	152	0·031	0·020
3	225	204	0·034	0·011

TABLE 3. Oscillation frequencies and damping at the measured critical flow velocities compared (for the shell without a splitter plate). The theoretical results were calculated with three-dimensional shell theory

$n = 2$, one obtains $U_c \simeq 17{\cdot}7$ m/s in the experiments, while theory gives $U_c \simeq 28{\cdot}7$ m/s, displaying a similar degree of discrepancy between theory and experiment as that in table 3.

7. Conclusion

In this paper a theory has been presented, based on the hypothesis that ovalling of shells in cross flow may be an aeroelastic phenomenon independent of any flow periodicity in the wake. The theoretical results have shown that:

(i) ovalling (flutter) may indeed be induced by the proposed mechanism;

(ii) flutter in the even- and odd-numbered circumferential modes occurs with a node and an antinode, respectively, facing the free stream;

(iii) the presence of a splitter plate results in slightly higher critical flow velocities, but otherwise-similar dynamical behaviour.

All of these theoretical predictions are in qualitative agreement with experimental observations; furthermore, for the shells tested, the modal sequence of the observed flutter, i.e. first in the second mode and then in the third, are as predicted by theory. However, quantitative agreement between predicted and measured thresholds of instability leaves a great deal to be desired, the onset of flutter being predicted only within a factor of 1·6 at best.

This lack of success of the theory, in terms of quantitative prediction, may be interpreted in two ways: either the fundamental hypothesis made is incorrect; or it is correct, but certain aspects of the theoretical model are insufficiently refined. The authors tend to believe the latter, in view of the extent of qualitative agreement with observed behaviour. Some aspects of the theoretical model which could usefully be tested are: (*a*) whether the mean velocity distribution and the location of the separation point are affected insignificantly by shell deformation and surface accelerations; (*b*) whether shell deformations (changes in shape) and mean stresses induced by the mean flow field have a negligible effect on the onset of flutter. These are currently under investigation.

The authors are grateful to Professor S. J. Price for many useful discussions and suggestions, to Professor B. G. Newman for constructive criticism of various aspects of this work and for making available the facilities of the Low-Speed Aerodynamics Laboratory, and to Mr Hon-Ching Suen of the same Department for allowing them to present some of his experimental and theoretical results. The authors also acknowledge the Natural Sciences and Engineering Research Council of Canada and Le Programme FCAC of Québec for the financial support which has made this research possible.

Appendix. Flutter analysis for ovalling with a node facing the free stream

If a node is situated at $\theta = 0$, then

$$\frac{\partial w^*}{\partial t} = 0.$$

Utilizing the fact that $f(0) = 0$, (3) and (4) reduce to

$$\left.\frac{\partial \phi_e^*}{\partial r}\right|_{r=a,\,\theta=0} = \left.\frac{\partial \phi_i^*}{\partial r}\right|_{r=a,\,\theta=0} = 0.$$

Consequently, this leads to

$$\phi_e^* = e^{i\omega t} \sum_{\lambda=1}^{\infty} D(\lambda)\, r^{-\lambda} \sin \lambda\theta,$$

$$\phi_i^* = e^{i\omega t} \sum_{\lambda=1}^{\infty} D(\lambda)\, r^{\lambda} \sin \lambda\theta.$$

Hence w^* and v^* in this case are expanded in the form

$$w^* = e^{i\omega t} \sum_{l=0}^{\infty} B_l \sin (2l+1)\, n\theta,$$

$$v^* = e^{i\omega t} \sum_{l=0}^{\infty} A_l \cos (2l+1)\, n\theta,$$

and the problem may be solved in the same manner as in § 3.

REFERENCES

Blevins, R. D. 1979 *Formulas for Natural Frequency and Mode Shape*, p. 309. Van Nostrand Reinhold.

Dickey, W. L. & Woodruff, G. B. 1956 *Trans. A.S.C.E.* **121**, 1054.

Dockstader, E. A., Swiger, W. F. & Ireland, E. 1956 *Trans. A.S.C.E.* **121**, 1088.

Dowell, E. H. 1975 *Aeroelasticity of Plates and Shells*, p. 20. Noordhoff.

Ewins, D. J. 1975 *J. Soc. Environ. Engrs* **14**, 3.

Flügge, W. 1957 *Statik und Dynamik der Schalen*, 2nd edn. Springer.

Goldstein, S. 1952 *Modern Developments in Fluid Dynamics*. Clarendon.

Johns, D. J. & Sharma, C. B. 1974 *Flow-induced Structural Vibrations*, p. 650. Springer.

King, R., Prosser, M. J. & Johns, D. J. 1973 *J. Sound Vib.* **29**, 169.

Lamb, H. 1957 *Hydrodynamics*, 6th edn, p. 19, § 20. Cambridge University Press.

Maskell, E. C. 1965 *A.R.C. R. & M.* no. 3400.

Paidoussis, M. P. & Helleur, C. 1979 *J. Sound Vib.* **63**, 527.

Parkinson, G. V. & Jandali, T. 1969 *J. Fluid Mech.* **40**, 577.

Ray, J. D., Bert, C. W. & Egle, M. D. 1969 *Shock Vib. Bull.* **39**, 107.

Roshko, A. 1954 *N.A.C.A. Tech. Note* no. 3169.

Scanlan, R. H. 1981*a* In *Proc. A.I.A.A./A.S.M.E./A.S.C.E./A.H.S. 22nd Structural Dynamics and Materials Conf., Atlanta, Georgia*, paper AIAA-81-0592-CP.

Scanlan, R. H. 1981*b* On aeroelastic mechanisms: Takoma Narrows 1940 (unpublished manuscript).

Suen, H.-C. 1981 *Ovalling vibration of cylindrical shells in cross flow*. M.Eng. thesis, McGill University.

Wygnanski, I. & Newman, B. G. 1961 *Aero. Section Mech. Eng. Res. Lab., McGill University, Rep. Ae*4.